J|A|C|S
ARTICLES
Published on Web 01/25/2006

Electronic Structure of Binuclear Mixed Valence Copper Azacryptates Derived from Integrated Advanced EPR and DFT Calculations

Shifra Kababya,[†] Jane Nelson,[‡] Carlos Calle,[||] Frank Neese,[§] and Daniella Goldfarb*,[†]

Contribution from the Department of Chemical Physics, Weizmann Institute of Science, Rehovot, Israel, Chemistry Department, Loughborough University, Leicester, UK, Max-Planck Institute for Bioinorganic Chemistry, Mülheim an der Ruhr, Germany, and Physical Chemistry Laboratory, ETH, Zürich, Switzerland

Received September 22, 2005; E-mail: daniella.goldfarb@weizmann.ac.il

Abstract: Binuclear, mixed valence copper complexes with a [$Cu^{+1.5}$, $Cu^{+1.5}$] redox state and $S = {}^1/_2$ can be stabilized with rigid azacryptand ligands. In this system the unpaired electron is delocalized equally over the two copper ions, and it is one of the very few synthetic models for the electron mediating Cu_A site of nitrous oxide reductase and cytochrome *c* oxidase. The spatial and electronic structures of the copper complex in frozen solution were obtained from the magnetic interactions, namely the *g*-tensor and the ^{63,65}Cu, ^{14}N, ^{2}H, and ^{1}H hyperfine couplings, in combination with density functional theory (DFT) calculations. The magnetic interactions were determined from continuous wave (CW) electron paramagnetic resonance (EPR), pulsed electron nuclear double resonance (ENDOR), two-dimensional TRIPLE, and hyperfine sublevel correlation spectroscopy (HYSCORE) carried out at W-band or/and X-band frequencies. The DFT calculated *g* and Cu hyperfine values were in good agreement with the experimental values showing that the structure in solution is indeed close to that of the optimized structure. Then, the DFT calculated hyperfine parameters were used as guidelines and starting points in the simulations of the various experimental ENDOR spectra. A satisfactory agreement with the experimental results was obtained for the ^{14}N hyperfine and quadrupole interactions. For ^{1}H the DFT calculations gave good predictions for the hyperfine tensor orientations and signs, and they were also successful in reproducing trends in the magnitude of the various proton hyperfine couplings. These, in turn, were very useful for ENDOR signals assignments and served as constraints on the simulation parameters.

Introduction

The mixed valence binuclear copper center Cu_A serves as an efficient electron mediator in nitrous oxide reductase (N_2OR) and a number of cytochrome *c* oxidases (COX).[1] Early multifrequency EPR experiments[2] and later several crystal structures[3−6] have shown that the two coppers are connected via cysteine thiolate bridges with a Cu−Cu separation of 2.5−2.6 Å. In addition, to each of the copper ions an imidazole group of a histidine residue is coordinated along with a weak axial ligand, usually a methionine sulfur and a main chain carbonyl oxygen of glutamine. In the oxidized state both copper atoms assume a formal oxidation state of 1.5 with a total spin $S = {}^1/_2$ delocalized over the Cu_2S_2 core with a spin population of up to 25% on the sulfurs. The unique structural and spectroscopic properties of Cu_A have motivated the synthesis of model compounds, which can reproduce the magnetic properties of this unique copper center. While binuclear mixed valence copper complexes do not form spontaneously without steric enforcement, they can form within a host which imposes on the copper ions bonding orbitals a proximity of ∼2.5 Å in a symmetrical coordination environment which is acceptable to both +1 and +2 oxidation states. So far two families of ligands that can stabilize a symmetric mixed valence Cu−Cu complex have been reported. One is the tridentate N_2S ligand $SCH_2CH_2(N_2C_6H_{12})CH(CH_3)_2^-$, which produces a complex with thiolate bridges, similar to Cu_A.[7] The second type comprises a series of octa-azacryptand macrocyclic ligands.[8−10] Although they form mixed valence Cu−Cu compounds with one unpaired electron delocalized over

[†] Weizmann Institute of Science.
[‡] Loughborough University
[§] Max-Planck Institute for Bioinorganic Chemistry
[||] ETH.

(1) Kroneck P. M. H. In *Handbook of Metalloproteins*; Messerschmidt, A., Huber, R., Poulos, T., Wieghart, K., Eds.; John Wiley and Sons: NY, 2001; Vol. 2, pp 1333−1341.
(2) Kroneck, P. M. H.; Antholin, W. E.; Kastraul, D. H. W.; Buss, G.; Steffens, G. C. M.; Zumft, W. G. *FEBS Lett* **1990**, *268*, 274−276.
(3) Wilmanns, M.; Lappalainen, P.; Kelly, M.; Saureriksson, E.; Saraste, M. *Proc. Natl. Acad. Sci. U.S.A.* **1995**, *92*, 11955−11959.
(4) Iwata, S.; Ostermeier, C. O.; Ludwing, B.; Michel, H. *Nature* **1995**, *376*, 660−669.
(5) Tsukihara, T.; Aoyama, H.; Yamashita, E.; Tomizaki, T.; Yamoguchi, H.; Shinzawa-Itoh, K.; Nakashima, R.; Yaonon, R.; Yoshikawa, S. *Science* **1995**, *269*, 1069−1074.
(6) Brown, K.; Tegoni, M.; Prudencio, M.; Pereira, A. S.; Besson, S.; Moura, J. J.; Moura, I.; Cambillau, C. *Nat. Struct. Biol.* **2000**, *7*, 191−195.
(7) Houser, R. P.; Young, V. G., Jr.; Tolman, W. B. *J. Am. Chem. Soc.* **1996**, *118*, 2101−2102
(8) Hardding, C. J.; McKee, V.; Nelson, J. *J. Am. Chem. Soc.* **1991**, *113*, 9684−9685.

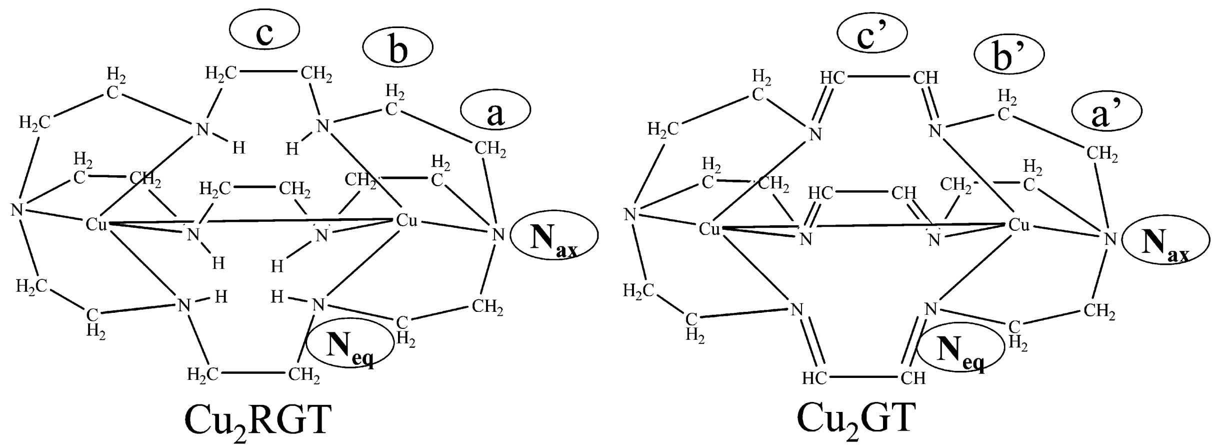

Figure 1. Schematic of Cu_2RGT and Cu_2GT. For label explanations see text.

the two copper atoms and a Cu−Cu distance of 2.45 Å,[11] compared to 2.43 Å in N_2OR, their electronic structure is significantly different. In Cu_A the SOMO is primarily a mixture between the Cu $d_{x^2-y^2}$ and the sulfur p orbital, forming a π type bonding with a small direct Cu−Cu overlap and significant spin density on the sulfur bridges.[12−14] In contrast, in the azacryptand complexes, the SOMO has d_{z^2} character, and the overlap between the d_{z^2} orbitals results in a relatively strong Cu−Cu σ bond with a much smaller electron delocalization over the bridging ligands, as determined by Raman spectroscopy.[10,15] Spectroscopic and theoretical studies that compared the Cu_A site with the thiolate based mixed valence synthetic model suggest that some structural elements are crucial for obtaining the electronic structure which optimizes the ET efficiency of the site.[16] Among these are the Cu-axial ligand distance and the orientation of the histidine ligand relative to the Cu−Cu axis. Moreover, the covalency of the Cu−S bonds has been considered an important factor in determining ET pathways.

In a recent study the proton hyperfine couplings of a number of Cu_A sites with known structures have been compared in order to rationalize their minor structural differences in terms of electronic structure, which in turn may be related to differences in activity.[17] It was found that the system is too complicated and the differences observed in the spin-distribution over the site could not be related to a single structural element. It was therefore suggested that density functional theory (DFT) could be applied in order to provide a clear correlation between the various structural elements and the electronic structure, based on reproducing the hyperfine interaction of as many nuclei as possible in the site. This motivated us to apply and test this approach using a simpler system, the binuclear copper complexes with the azacryptand ligands. DFT calculations of spin Hamiltonian parameters have been shown to be an important tool in the interpretation of experimental EPR data in terms of both assignment and derivation of structures.[18,19] Nonetheless, the ability of the DFT to predict hyperfine couplings strongly depends on obtaining an optimized structure that is similar to the real structure, as shown in a recent detailed study on Cu(II)−histidine complexes in aqueous solutions.[20]

In this work the two copper complexes shown in Figure 1 are investigated in depth. They are based on two azacryptand ligands, RGT and GT reported previously.[8−10] Both have a rigid structure which consequently is expected to be similar in solution and in the crystal. Therefore the issue of the relation between the optimized structure and the real structure should be of a lesser concern, allowing us to evaluate how well DFT calculations can predict hyperfine interactions. We have concentrated primarily on the Cu_2RGT structure, whereas the Cu_2GT structure was used mostly for assignment purposes. ^1H, ^2H, and ^{14}N hyperfine couplings were determined by W-band (94.9 GHz) electron−nuclear double resonance (ENDOR) spectroscopic techniques, complemented by X-band ENDOR and HYSCORE (hyperfine sublevel correlation) spectroscopy. In addition, we have used two-dimensional (2D) TRIPLE experiments to determine the extent of the ^1H hyperfine anisotropy and the relative signs of the hyperfine couplings. The DFT calculations were essential for the assignment of the signals; they provided important guidelines for spectral simulations of the ENDOR spectra and gave the rationale for the spin density distribution. In general a good agreement was obtained between the experimental and calculated g-tensor and the Cu and ^{14}N hyperfine interactions. For the proton hyperfine couplings the agreement for orientations, signs, and trends was found to be good, while the prediction of the absolute values was not always satisfactory. Thus, this study represents a careful benchmark study of what can presently be achieved in the experimental

(9) Harding, C. J.; Nelson, J.; Symons, M. C. R.; Wyatt, J. *J. Chem. Soc., Chem. Commun.* **1994**, 2499−2500.
(10) Farrar, J.; McKee, V.; Al-Obaidi, A. H. R.; McGarvey, J. J.; Nelson, J.; Thomson, A. *Inorg. Chem.* **1995**, *34*, 1302−1303.
(11) Charnock, J. M.; Dreusch, A.; Korner, H.; Neese, F.; Nelson, J.; Kannt, A.; Michel, H.; Garner, C. D.; Kroneck, P. M. H.; Zumft, W. G. *Eur. J. Biochem.* **2000**, *267*, 1368−1381.
(12) Neese, F.; Zumft, W. G.; Antholine, W. E.; Kroneck, P. M. H. *J. Am. Chem. Soc.* **1996**, *118*, 8692−8699.
(13) Farrar, J.; Neese, F.; Lappalainen, P.; Kroneck, P. M. H.; Saraste, M.; Zumft, W. G.; Thomson, A. J. *J. Am. Chem. Soc.* **1996**, *118*, 11501−11514.
(14) Neese, F.; Kappl, R.; Zumft, W. G.; Hüttermann, J.; Kroneck, P. M. H. *J. Biol. Inorg. Chem.* **1998**, *1*, 53−67.
(15) Farrar, J.; Grinter, R.; Neese, F.; Nelson, J.; Thomson, A. *J. Chem. Soc., Dalton Trans.* **1997**, 4083−4087.
(16) Gamelin, D. R.; Randall, D. W.; Hay, M. T.; Houser, R. P.; Mulder, T. C.; Canters, G. W.; de Vries; Tolman, W. B.; Lu, Y.; Solomon, E. I. *J. Am. Chem. Soc.* **1998**, *120*, 5246−63.
(17) Epel, B.; Slutter, C. S.; Neese, F.; Kroneck, P. M. H.; Zumft, W. G.; Pecht, I.; Farver, O.; Lu, Y.; Goldfarb, D. *J. Am. Chem. Soc.* **2002**, *124*, 8152−8162.
(18) Baute, D.; Goldfarb, D. *J. Phys. Chem. A* **2005**, *109*, 7865−7871.
(19) Neese, F. *Curr. Opin. Chem. Biol.* **2003**, *7*, 125−135.
(20) Baute, D.; Arieli, D.; Neese, F.; Zimmerman, H.; Weckuysen, B. M.; Goldfarb, D. *J. Am. Chem. Soc.* **2004**, *126*, 11733−11745.

and theoretical investigations of magnetic resonance parameters of transition metal complexes.

Experimental Section

Samples. $[Cu_2RGT](BF_4)_3$, $[Cu_2RGT](ClO_4)_3$, and $[Cu_2\ GT](ClO_4)_3$ were prepared as described earlier.[8,21] The W- and X-band samples' concentration was 1 mM of the complex in a 1:1 water glycerol solution. The solutions were loaded into 3 mm and 0.84 mm o.d. quartz tubes, respectively, which were immediately frozen to 77 K to minimize decomposition. Samples were prepared also in a 1:1 D_2O and deuterated glycerol ($CHOD(CH_2OD)_2$), Cambridge Isotope Laboratories Inc.) solutions.

Spectroscopic Measurements. W-band pulsed EPR and ENDOR measurements were carried out at 94.9 GHz and 6.5−8.5 K on a home-built spectrometer described elsewhere.[22] Field-sweep (FS) echo-detected (ED) EPR spectra were recorded using the two-pulse echo sequence (π/2-τ-π-τ-echo), where the echo intensity is registered as a function of the magnetic field. Typically, microwave (MW) pulse lengths, t_{MW}, of 90 and 180 ns were used with $\tau = 0.3$ or 0.4 μs and a 10 ms repetition time. The magnetic field values were calibrated using the Larmor frequency of the protons, ν_H, as determined by the ENDOR measurements. The ^{1}H ENDOR spectra were measured using the Davies ENDOR pulse sequence (π-T-π/2-τ-π-τ-echo, with an RF π pulse applied during the time interval T) with $t_{MW} = 0.2$, 0.1, 0.2 μs, respectively, $\tau = 0.3$ μs. The RF pulse length, t_{RF}, was 10 μs, and T was 15 μs. The Mims ENDOR sequence (π/2-τ-π/2-T-π/2-τ-echo, with an RF π pulse applied during the time T) was used for the ^{2}H ENDOR measurements with $t_{MW} = 0.1$ μs, $\tau = 0.4$ μs, and $t_{RF} = 30$ μs. The intensity and frequency scales of the ^{2}H spectra were multiplied by −1 and γ^H/γ^D (=6.5144), respectively, to allow a convenient comparison with the ^{1}H ENDOR spectra. The frequency scale in the ^{1}H and ^{2}H ENDOR spectra is given with respect to the Larmor frequency $\nu = \nu_{RF} - \nu_H$. The 2D TRIPLE experiment[23] was performed using a pulse sequence similar to that of the Davies ENDOR, where a second RF π pulse is applied 0.2 μs after the first RF pulse using the same pulse durations as those in the Davies ENDOR measurements but with $T = 25$ μs. The 2D data were collected by measuring the echo intensity as a function of the frequencies of the first and second RF pulses, and the total number of points was 100 × 100. A total of 30 shots were accumulated for each point. The 2D spectrum was obtained by subtracting from each trace the normal ENDOR spectrum.

X-band pulsed EPR, ENDOR, and HYSCORE measurements were carried out at 9.77 GHz and 8 K on an Elexsys E-580 Bruker spectrometer. The ENDOR spectra were measured using the Davies ENDOR pulse sequence with $t_{MW} = 0.06$, 0.03, 0.06 μs, respectively, $\tau = 0.2$ μs and $t_{RF} = 14$ μs. For the HYSCORE pulse sequence (π/2-τ-π/2-t_1-π-t_2-π/2-τ-echo) $t_{MW} = 0.024$ μs was used for all pulses and a four step phase cycle was applied. The dwell time in t_1 and t_2 was 0.024 μs, and 120 × 120 points were collected with $\tau = 0.16$ μs and 0.2 μs, a repetition time of 5 ms, and 100 shots per point.

Spectral Simulations. EPR simulations were carried out using a previously reported program.[24] The ENDOR simulations were performed using an in-house program and the Kazan tool box,[25] which is based on EasySpin,[26] 2D TRIPLE spectra were simulated using an in house written program also based on EasySpin,[27] and the HYSCORE spectra were calculated using TRYSCORE.[28] The g-tensor was assumed as axial with the direction of $g_{||}$ along the Cu−Cu bond, based on the DFT calculations and our experimental results. The selected orientations in the orientation selective ENDOR measurements were determined graphically from the road map of the simulated EPR spectrum which gives the resonant magnetic fields as a function of the angle θ_0,[29] assuming an inhomogeneous line width of 45 G.

Computational Details. All calculations were done with the ORCA electronic structure package version 2.4.26.[30] Two sets of calculations were carried out. The first set of calculations were based on the experimental structures with coordinates directly taken from the X-ray diffraction experiments.[21] The second set of calculations was done on geometry optimized structures. The geometry optimizations were done in redundant internal coordinates without constraints. The BP86 functional[31,32] together with a polarized triple-ζ quality basis set (TZV)[33] was used in these calculations, and the Coulomb term was approximated with the resolution-of-the-identity (RI) approximation to gain computational efficiency.[34] The metal basis was supplemented with 2p and 1f polarization functions, while the carbon and nitrogen bases were supplemented with a single d-set. The hydrogen basis set was left unpolarized in these calculations. All exponents of polarization functions were taken from the TurboMole library.[36] The auxiliary basis sets were taken from the work of Eichkorn et al.[34] and were chosen to match the orbital basis. Following previous experience, the calculation of EPR properties was done using the B3LYP hybrid functional which leads to somewhat better EPR property predictions for transition metal complexes compared to GGA functionals.[37−40] In these calculations much more extensive basis sets were used. The copper ions were described with the CP(PPP) basis (17s5p3d) documented previously[35] which is based on the Ahlrichs DZ basis set[36] but has additional flexibility in the core region. The nitrogen atoms were described with the IGLO-III basis[41] (7s6p2d), the carbon atoms, with the TZVP basis (5s3p1d), and the hydrogen atoms, with the EPR-II basis (6s2p).[42] Altogether this leads to 1050−1150 basis functions. Accurate numerical integration of the exchange-correlation potential in the presence of steep basis functions was ensured.

The g-tensor was calculated through solution of the coupled-perturbed Kohn−Sham equations.[38] The origin was chosen as the center of electronic charge.[43] The calculations include the relativistic mass correction, diamagnetic spin−orbit, and paramagnetic spin−orbit terms. The former (small contribution) was evaluated through an empirically parametrized spin−orbit operator which features effective nuclear charges.[44] The dominant paramagnetic SOC (spin−orbit coupling) term

(21) Al-Obaidi, A. H. R.; Baranovich, G.; Coates, C.; Coyle, J.; McGarvey, J. J.; McKee, V.; Nelson, J. *Inorg. Chem.* **1998**, *37*, 3567−3574.
(22) Gromov, I.; Krymov, V.; Manikandan, P.; Arieli, D.; Goldfarb, D. *J. Magn. Reson.* **1999**, *139*, 8−17.
(23) Epel, B.; Goldfarb, D. *J. Magn. Res.* **2000**, *146*, 196−203.
(24) Neese, F. Electronic Structure and Spectroscopy of Novel Copper Chromophores in Biology. Ph.D. Thesis, University of Konstanz, 1997.
(25) Epel, B. http://www.geocities.com/boep777/.
(26) Stefan Stoll. Spectral Simulations in Solid-State EPR. Ph.D. Thesis, ETH Zurich, 2003 (http://www.easyspin.ethz.ch/).
(27) Goldfarb, D.; Epel, B.; Zimmermann, H.; Jeschke, G. *J. Magn. Reson.* **2004**, *168*, 75−87.
(28) Szosenfogel, R.; Goldfarb, D. *Mol. Phys.* **1998**, *95*, 1295−1308.
(29) Goldfarb, D.; Fauth, J. M.; Tor, Y.; Shanzer, A. *J. Am. Chem. Soc.* **1991**, *113*, 1941−1948.
(30) Neese, F. *ORCA−an ab initio, Density Functional and Semiempirical Program Package*, version 2.4, revision 26; Max Planck Institut für Bioanorganische Chemie: Mülheim an der Ruhr, 2004.
(31) Becke, A. D. *Phys. Rev. A* **1988**, *38*, 3098−3100.
(32) Perdew, J. P. *Phys. Rev. B* **1986**, *33*, 8822−8824.
(33) Schäfer, A.; Huber, C.; Ahlrichs, R. *J. Chem. Phys.* **1994**, *100*, 5829−5835.
(34) Eichkorn, K.; Weigend, F.; Treutler, O.; Ahlrichs, R. *Theor. Chem. Acc.* **1997**, 97, 119−124. Eichkorn, K.; Treutler, O.; Öhm, H.; Häser, M.; Ahlrichs, R. *Chem. Phys. Lett.* **1995**, *240*, 283−290.
(35) Neese, F. *Theor. Inorg. Chim. Acta* **2002**, *337*, 181−192.
(36) Ahlrichs, R. and co-workers, 2001, ftp.chemie.uni-karlsruhe.de/pub/basen.
(37) Neese, F. *J. Phys. Chem. A* **2001**, *105*, 4290−4299.
(38) Neese, F. *J. Chem. Phys.* **2001**, *115*, 11080−11096.
(39) Neese, F. *J. Chem. Phys.* **2003**, *118*, 3939−3948.
(40) Kaupp, M.; Reviakine, R.; Malkina, O. L.; Arbuznikov, A.; Schimmelpfennig, B.; Malkin, V. *J. Comput. Chem.* **2001**, *23*, 794−803. Neese, F. *Inorg. Chim. Acta* **2002**, *337*, 181−192.
(41) Kutzelnigg, W.; Fleischer, U.; Schindler, M. In *NMR basic principles and progress*; Diehl, P., Fluck, E., Günther, H., Kosfield, R., Seeling, J., Eds.; Springer: Heidelberg, 1990.
(42) Barone, V. In *Recent Advances in Density Functional Methods (Part I)*; Chong, D. P., Ed.; World Scientific Publishing Co.: 1995; Chapter 8, pp 287−334.
(43) Luzanov, A. V.; Babich, E. N.; Ivanov, V. V. *THEOCHEM* **1994**, *311*, 211−220.
(44) Koseki, S.; Schmidt, M. W.; Gordon, M. S. *J. Phys. Chem.* **1992**, *96*, 10768−10772.

Scheme 1

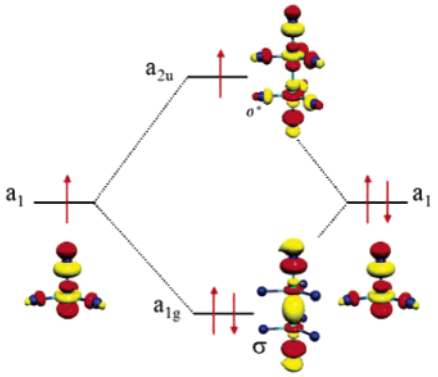

was calculated with the recently reported,[45] accurate multicenter implementation of the spin−orbit mean-field (SOMF) concept.[46] The spin−orbit Coulomb term was approximated with the RI approximation using automatically generated fitting bases, while the much smaller exchange terms were treated in the one-center approximation (RI-SOMF(1X)).[45] The copper hyperfine coupling calculations include the Fermi-contact term, the spin-dipolar contribution, and the SOC correction. The latter was again calculated by coupled-perturbed Kohn−Sham theory as described earlier[39] but with the difference that the SOC operator was the same RI-SOMF(1X) operator used in the *g*-tensor calculations. The calculations of the nitrogen and hydrogen hyperfine and quadrupole tensors only included the first-order terms, since based on the previous experience SOC corrections are small for light ligand nuclei in such complexes.[37]

Results

In the following the experimental EPR/ENDOR and the DFT calculation results will be presented together rather than consecutively because this format illustrates how the two were integrated for achieving a concise interpretation of the experimental results.

Structure and Bonding. The overall electronic structure of the compounds studied is well-known[10,15,24] and will only be briefly recalled in order to facilitate the discussion. It is instructive to start from two C_{3v} symmetric trigonal pyramidal fragments. Basic ligand field theory dictates that in such a coordination geometry the highest energy d-orbital is the Cu-d_{z^2} orbital. Upon bringing together two such fragments along the molecular *z*-axis, the two lobes of the d_{z^2} orbitals can strongly overlap and form a standard two-center metal−metal bond. However, in the present case, there are three electrons to be distributed over the bonding and antibonding components of this bond, thus leaving a net copper−copper bond of formal bond order $^1/_2$ (Scheme 1).

In terms of standard mixed-valence theory,[47] the transition $\sigma \rightarrow \sigma^*$ ($^2A_{1g} \rightarrow {}^2A_{2u}$) corresponds to twice the intersite electronic matrix element H_{AB}. Based on MCD (magnetic circular dichroism) and absorption studies, this transition has been assigned to the very intense absorption and reasonably weak MCD band at ~13 000 cm^{-1}.[12] Thus, the interelectronic interaction between the two copper fragments is very large and easily overcomes the vibronic trapping energy which provides a satisfactory rationale for its delocalized class III mixed valence behavior.

(45) Neese, F. *J. Chem. Phys.* **2005**, *122*, 34107−34113.
(46) Hess, B. A.; Marian, C. M.; Wahlgren, U.; Gropen, O. *Chem. Phys. Lett.* **1996**, *251*, 365−371.
(47) Schatz, P. N. In *Mixed Valence Compounds*; Brown, R. D., Ed.; D. Reidel Pub.: 1980; pp 115−150.

Table 1. Comparison of Key Calculated and X-ray Determined Experimental (in Parentheses) Structure Parameters for the Two Complexes Studied in This Work

distance, Å	Cu_2RGT	Cu_2GT
Cu−Cu	2.464 (2.379)	2.514 (2.380)
$Cu-N_{ax}$[a]	2.110 (2.071)	2.147 (2.041)
$Cu-N_{eq}$[a]	2.129 (2.039)	2.024 (1.959)

[a] The experimental structure parameters for Cu−N were averaged in order to facilitate the comparison.

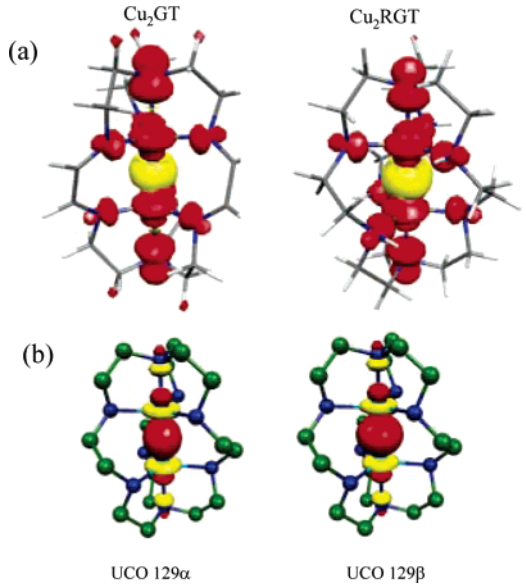

Figure 2. (a) Spin density of $[Cu_2(RGT)]^{3+}$ and $[Cu_2(GT)]^{3+}$ at a contour level of 0.002 (dark gray = positive, light gray = negative) and (b) the spin-polarized corresponding orbital pair for $[Cu_2RGT]^{3+}$, which corresponds to the σ Cu−Cu bonding interaction (contour level 0.05 (electrons/bohr)$^{1/2}$). Spin polarization of this orbital leads to the negative spin density in the bonding region observed in part (a) of the figure. All contours were obtained from B3LYP calculations with the large basis set described under the experimental section.

A detailed assignment of the optical transitions has been worked out previously,[10,15,24] and additional valuable information has been extracted from resonance Raman spectroscopy.[21]

The present study focuses on the details of the geometric and electronic structure of the electronic ground state. The most important calculated structural parameters are compared with the values deduced from X-ray diffraction in Table 1. At a first glance it appears that the DFT results are only in moderate agreement with the experimental data. In particular, the Cu−N distances are all overestimated. However, it should by noted that the experimental diffraction data for Cu_2RGT show a spread of almost 0.1 Å in the equatorial Cu−N distances which perhaps points to a problem with the structure determination. Based on previous experience it is likely that the DFT results overestimate the Cu−N distances by about 0.05−0.1 Å. A more definitive conclusion cannot be drawn on the basis of the experimental data. The situation is different for Cu_2GT where the experimental data show a high degree of consistency. Here, the same behavior is noted: the DFT predicted bond distances are too long by about 0.05−0.1 Å. Since these deviations represent unusually large deviations, we decided to base the property calculations on both the optimized and the experimental coordinates, as will be further discussed below.

Figure 2 shows the calculated spin densities in Cu_2RGT and Cu_2GT along with the spin-polarized corresponding orbital pair

for $[Cu_2RGT]^{3+}$, which corresponds to the σ Cu−Cu bonding interaction. It is evident, that the overall features of the spin density are rather similar in the two compounds and do not warrant separate discussion. The spin density is dominated by the contribution from the SOMO. This orbital is, as expected, formed from the antibonding d_{z^2} combination of the two copper ions with substantial covalent admixtures from the nitrogen ligands. Naturally, the capping nitrogens make a larger contribution to the SOMO and therefore also carry more spin population than the equatorial nitrogen ligands.

One curious feature of the spin density in these compounds is the occurrence of a region of negative spin density located around the midpoint of the copper−copper bond. We have not observed such a spin-polarization phenomenon in previous calculations on mixed valence species. Since the spin-unrestricted B3LYP DFT calculations give no sign of excessive problems with spin contamination ($\langle S^2 \rangle \approx 0.77$ compared to 0.75 expected for a pure doublet state), we have tried to trace back the origin of this effect by studying the unrestricted corresponding spin−orbitals. In this method the spin-up and spin-down molecular orbitals are separately subjected to a unitary transformation such that each spin-up MO has a nonzero spatial overlap with at most one spin-down MO. Thus, MO pairs of maximum similarity are produced by the transformation, and a spatial overlap of substantially less than unity indicates a significant spin-polarization contribution from this particular MO pair. The one unmatched spin-up MO corresponds precisely to the exactly singly occupied natural orbital of the spin unrestricted wave function. A detailed inspection of the calculated pairs indicates that with one exception all formally doubly occupied pairs have overlaps of at least 0.999 and are therefore very little spin polarized. However, a single pair has only an overlap of 0.988. As seen in Figure 2b, this pair corresponds to the formally doubly occupied Cu−Cu bonding orbital. Upon inspection, it is observed that the spin-down component is more spatially extended in the bonding region than the spin-up component which thus explains the observed negative spin density in this region. Physically, this effect may be regarded as a consequence of the virial theorem as analyzed long ago by several workers.[48−51] To maintain the balance between potential and kinetic energy, atomic orbitals which contribute to bonding molecular orbitals tend to expand, while those contributing to antibonding molecular orbitals tend to contract. Since, in the spin-up manifold, the bonding and antibonding components of the Cu−Cu bond are occupied, there is a net balance. In the spin-down manifold, bonding can be maximized by letting the Cu-$3d_{z^2}$ radial functions expand which leads to the accumulation of electron density in the Cu−Cu bonding region and strengthens the Cu−Cu bond. Unfortunately, none of the observables studied in this work is particularly sensitive to the occurrence of negative spin density in the midpoint of the Cu−Cu bond, and thus, the effect cannot be put to an experimental test at this point. An experimental proof would probably require a detailed polarized neutron diffraction study which is outside the scope of the present work.

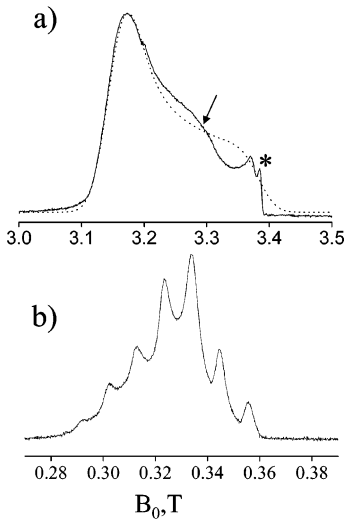

Figure 3. (a) W-Band FS-ED EPR spectrum of Cu_2 RGT in H_2O measured at 6.5 K. (b) The corresponding X-band ED-FS spectrum (8 K). The dotted line represents the simulated spectrum, * marks the $g = 2$ impurity, and the arrow points to the mononuclear Cu(II) complex.

EPR Spectra and the *g* and Copper Hyperfine Values. The W- and X-band FS-ED EPR spectra of a frozen solution of $Cu_2RGT(ClO_4)_3$ are shown in Figure 3a,b, respectively, and the same spectra were measured for $Cu_2RGT(BF_4)_3$. The measurements at two frequencies are complementary because the first resolves the *g*-anisotropy, while the second provides the Cu hyperfine couplings. The *g*-values obtained are in good agreement with those determined earlier by X-band EPR.[9] A simulated trace obtained with $g_\perp = 2.148$, $g_\| = 2.004$ is shown as well (dotted line). The spectrum has an additional feature, at $g = 2.02$, which is attributed to the $g_\perp$ of a mononuclear Cu(II) complex produced by the decomposition of the mixed valence complex. The intensity of this peak increased, when the sample was left at room temperature for a few weeks. In addition, a minor sharp signal appearing at $g = 2$ is evident. The origin of this signal is not clear, but because its relative intensity is very small it has been ignored. The W-band spectrum of $Cu_2GT(ClO_4)_3$ is similar; the radical impurity is absent, but the relative amount of the mononuclear Cu(II) is higher (not shown). Since the ENDOR results obtained from the BF_4^- and ClO_4^- salts were the same, for brevity the complexes will be referred to just as Cu_2RGT and Cu_2GT.

The experimental *g* and Cu hyperfine values are listed in Table 2 along with the DFT predicted values for the crystal and optimized structures. The agreement between the experimental and calculated values is surprisingly good, compared to earlier reports for mononuclear Cu(II) complexes.[37,39] The agreement seems somewhat better for the optimized structure than for the crystal structure for both types of complexes. Moreover, the agreement for Cu_2RGT is better than that for Cu_2GT. From group theory, it is evident that the $g_\|$ can only lie along the unique long axis which is defined by the Cu−Cu bond. This expectation is confirmed in the DFT calculations which predict the $g_\|$ component to occur within 0.5° of the Cu−Cu vector. Similarly, a very good agreement was obtained for the copper hyperfine couplings, where the deviation in $A_\|$ may arise from experimental uncertainty due to the small value. The good agreement with the experimental *g* and Cu hyperfine interaction lends confidence to the optimized structures. This is actually not surprising since the structure is very rigid.

(48) Ammeter, J. *Chimia* **1968**, *22*, 469−473 and Dissertation Eidgenössische Technische Universität Zürich 1969.
(49) Rüdenberg, K. *Rev. Mod. Phys.* **1962**, *34*, 326−376.
(50) Feinberg, M. J.; Rüdenberg, K.; Mehler, E. L. *Adv. Quantum Chem.* **1970**, *5*, 27−98.
(51) Feinberg, M. J.; Rüdenberg, K. *J. Chem. Phys.* **1971**, *59*, 1495−1511.

Table 2. Experimental *g* and Copper Hyperfine Values of Cu_2RGT and Cu_2GT and the DFT Calculated Values Obtained from the Optimized Structure and the Crystal Structure Coordinates

	$g_\perp$[a]	$g_\parallel$	$A^a(Cu)_\perp$, MHz	$A(Cu)_\parallel$, MHz
Cu_2RGT, exp	2.148	2.004	(−)308[b]	(+)10[b,9]
Cu_2RGT, DFT, crystal	2.1156/2.1214	2.0044	−272.7/−331.9	−5.3
Cu_2RGT, DFT, optimized	2.1376/2.1381	2.0033	−304.8/−306.2	0.3
Cu_2GT, exp	2.148	2.004	(−)308[b]	(+)10[b,9]
Cu_2GT, DFT, crystal	2.1071	2.0052	−286.6	20.0
Cu_2GT, DFT, optimized	2.1214	2.0055	−265.7	10.9

[a] When two values are listed they refer to the *xx* and *yy* components, respectively. [b] The sign was not determined experimentally but was taken from the calculations.

The observed *g*-values and copper hyperfine parameters can be used to obtain a qualitative estimate of the composition of the SOMO in these compounds and the necessary equations have been worked out previously.[24] Essentially, these are closely analogous to those for a mononuclear Cu(II) species with a $(d_{z^2})^1$ configuration with the obvious difference that the copper hyperfine couplings are scaled by a factor of $^1/_2$ in order to account for the delocalized mixed-valence nature of the ground state. Specifically, one obtains

$$A_\parallel(\mathrm{Cu}) = P_{3d}^{Cu}\left[-\kappa + \frac{4}{7}\delta^2 - \frac{1}{7}(g_\perp - g_e)\right]$$
$$A_\perp(\mathrm{Cu}) = P_{3d}^{Cu}\left[-\kappa - \frac{2}{7}\delta^2 - \frac{1}{14}(g_\perp - g_e)\right] \qquad (2)$$

where δ^2 is the fractional copper d_{z^2} character in the SOMO, κP_{3d}^{Cu} is the isotropic hyperfine coupling, and P_{3d}^{Cu} is a constant ($P_{3d}^{Cu} = g_e g_{Cu} \beta_e \beta_{Cu} \langle r^{-3} \rangle = 1134$ MHz). Using in this equation the experimental values $g_\perp = 2.148$, $A_\perp(\mathrm{Cu}) = 100$ G, and $A_\parallel(\mathrm{Cu}) = \pm 10$ G, we obtained $\delta = 0.76-0.78$, which corresponds to $\rho_{Cu} = 38-39\%$ on each copper ion. As expected, these estimates for the spin populations on the copper centers are somewhat higher than those calculated by DFT which amount to 33% on average. This effect has been analyzed many times previously[38,52−54] Based on the work of Patchkovskii et al.,[55] it appears that this is mainly a consequence of the self-interaction error which plagues all standard DFT functionals. Nevertheless, the agreement with the theoretically calculated spin populations (which, of course, do not represent physical observables) is fairly reasonable and allows one to proceed with the analysis to finer details of the spin density distribution.

Next we discuss the spin Hamiltonian parameters of the ^{14}N nuclei, some of which are predicted to have rather large spin populations, and therefore substantial hyperfine couplings are expected.

Nitrogen Hyperfine and Quadrupole Interactions. The symmetrical molecular structure of Cu_2RGT suggests the presence of two types of inequivalent nitrogens, the two capping (axial) nitrogens, referred to as N_{ax}, and the other six bridging equatorial nitrogen atoms termed N_{eq} (Figure 1). Here we applied W-band and X-band ENDOR for the detection of the strongly coupled nitrogen and X-band HYSCORE for the weakly coupled nitrogen, while the DFT results were used as guidelines pointing to the spectral region where signals are expected and for assignment. The ^{14}N W-band Davies ENDOR spectrum of Cu_2RGT/H_2O recorded at two magnetic field positions within the EPR powder pattern is shown in Figure 4. At 3.172 T, close to $g_\perp$, the spectrum exhibits two broad peaks at 13 and 16.5 MHz, with approximately the same intensity, and a sharper peak at 19 MHz. Upon shifting the field to the lowest field edge of the EPR spectrum, the 16 MHz line sharpens considerably. Unfortunately the spectrum measured at a field close to $g_\parallel$ suffered from poor *S*/*N*, and no clear signals could be detected. The observed spectra suggest that two types of ^{14}N nuclei are present, but because their line shapes are not distinctive enough we have carried out complementary X-band ENDOR and HYSCORE measurements.

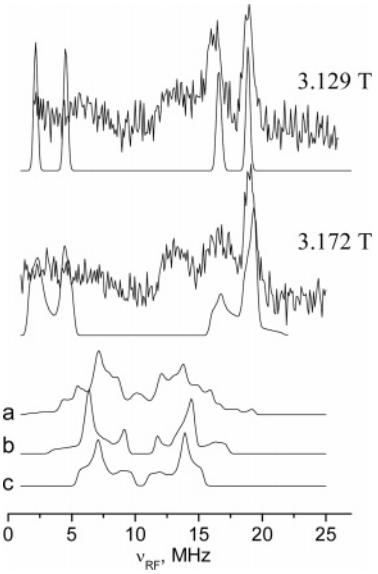

Figure 4. W-Band ^{14}N Davies ENDOR spectra of Cu_2RGT in H_2O recorded at different magnetic field positions (as noted on the figure) along with simulations. The top black solid lines are the simulated spectra of N_{ax} obtained with the parameters noted as N_{ax}(exp) in Table 3. The orientations selected for the simulations were 80°−90° and 60°−90° for θ_0 (top to bottom spectra, respectively) and 0°−180° for ϕ_0. The group of spectra marked with a, b, and c are the sum of all six simulated spectra of N_{eq} at 3.1723 T. (a, b) Calculated with the DFT values obtained from the crystal and optimized structure, respectively. (c) Calculated the parameters obtained from the HYSCORE simulation, noted as N_{eq}(exp) in Table 3. All parameters are listed in Table 3, and the a, b, and c traces were scaled to fit the amplitude of the 13 MHz peak.

The X-band Davies ENDOR spectra of Cu_2RGT recorded at different magnetic fields are shown in Figure 5. These reveal a ^{14}N doublet, split by $2\nu_I$, at 8 and 10 MHz that overlaps with a proton doublet in the field range 304.4−325 mT. An additional weak signal appears around 3 MHz. These spectra do not exhibit any orientation selection but the field dependence allowed to resolve of the ^{14}N and ^{1}H signals. Similar to the W-band results,

(52) Solomon, E. I. *Comments Inorg. Chem.* **1984**, *3*, 225−320.
(53) Solomon, E. I.; Lowery, M. D. In *The Chemistry of Copper and Zinc Triads*; Welch, A. J., Chapman, S. K., Eds.; Special Publication−Royal Society of Chemistry: 1993; Vol. 131, pp 12−29.
(54) Szylagyi, R. K.; Metz, M.; Solomon, E. I. *J. Phys. Chem. A* **2002**, *106*, 2994−3007.
(55) Patchkovskii, S.; Autschbach, J.; Ziegler, T. *J. Chem. Phys.* **2001**, *115*, 26−42.

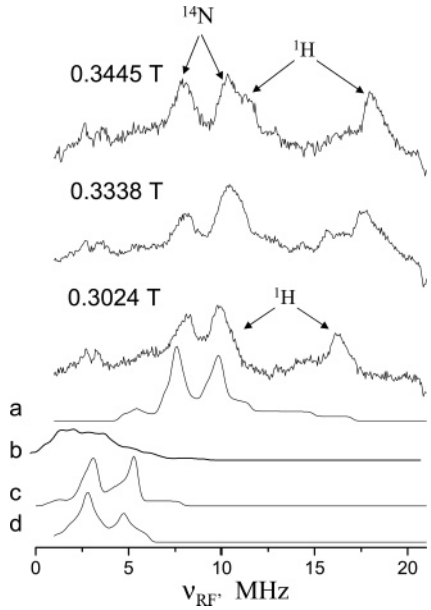

Figure 5. X-Band Davies ENDOR spectra of Cu_2RGT in H_2O spectra recorded at different magnetic field positions (as noted on the figure) along with simulations (a−d traces). (a) Represents the best fit simulated spectrum of N_{ax} obtained with the parameters noted as N_{ax}(exp) in Table 3. It was scaled to fit the experimental spectrum recorded at 0.3024 T. The b−d traces are calculated spectra of all six N_{eq} nuclei at 0.3024 T. (b,c) Calculated with the DFT values of the crystal and optimized structure, respectively. (d) Calculated with the parameters obtained from the HYSCORE simulation, noted as N_{eq}(exp) in Table 3. The orientations selected for the simulations were 0°−90°, and 0°−180° for θ_0 and ϕ_0, respectively. All parameters are listed in Table 3.

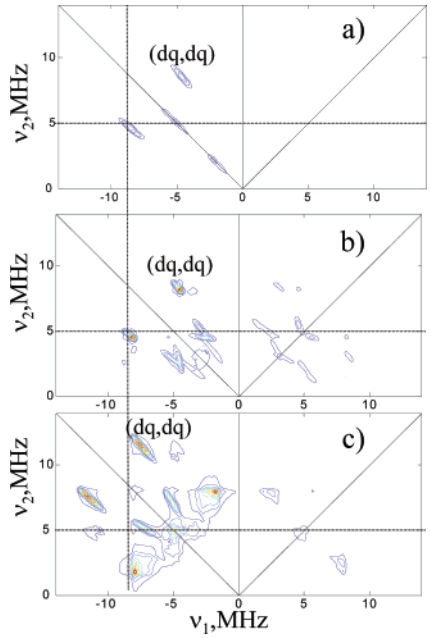

Figure 6. HYSCORE spectrum of Cu_2RGT recorded at $B_0 = 0.3455$ T and $\tau = 0.16$ μs. (b) Spectrum calculated with the parameters listed in Table 3 as N_{eq} (exp), and (c) spectrum calculated with DFT parameters of N_{eq} of the optimized structure (see Table 3). The (dq,dq) cross-peaks are labeled. All other peaks involve sq type transitions.

these spectra are consistent with two types of nitrogens with significantly different couplings. The HYSCORE spectra of this sample, shown in Figure 6a, exhibit a single pair of double quantum peaks (dq,dq) at (8.3, 4.7) in the (−, +) quadrant. Spectra recorded at 0.3455 and 0.3337 T at different τ values

Table 3. DFT Values of the Hyperfine and Quadrupole Tensors Components of the Nitrogen Nuclei of Cu_2RGT Obtained from the Optimized Structure and the Crystal Structure Coordinates Compared with the Experimental Values

nuclei type and no.	A_{xx}, MHz	A_{yy}, MHz	A_{zz}, MHz	β, γ (deg)	e^2Qq/h, MHz	η	β', γ' (deg)
Crystal							
N_{ax}, 2[a]	14.6	14.9	33.0	2, 0	−3.9175	0.27	0, 0
N_{ax}, 25	13.1	13.2	31.4	1, 106	−4.0859	0.11	2.7, 15
N_{eq}, 9	3.1	3.3	7.0	101, 272	−3.48	0.35	78, 274
N_{eq}, 32	3.4	3.5	7.5	76, 262	−3.44	0.38	79, 276
N_{eq}, 62	3.6	3.8	8.1	78, 262	−3.49	0.35	75, 278
N_{eq}, 40	3.8	4.1	8.1	104, 260	−3.30	0.24	102, 268
N_{eq}, 17	6.0	6.2	11.6	76, 267	−3.20	0.19	72, 102
N_{eq}, 54	7.6	7.8	13.6	106, 264	−3.14	0.30	101, 276
Optimized							
N_{ax}	14.3	14.3	31.5	0, 180	−4.0	0.0	0, 90
N_{eq}	5.1	5.2	9.8	105, 270	−3.4	0.15	75, 275
N_{ax} (exp)	14.5	14.5	26.5	0, 10	−3.7	0.3	0, 0
N_{eq} (exp)	5.5	5.5	7	0, 0	3.0	1	0, 0

[a] The number corresponds to the atom number in the structure in the Supporting Information.

were similar. Simulations showed that such spectra can be reproduced by one ^{14}N nucleus with $(A_{xx},A_{yy},A_{zz}) = 5.5, 5.5, 7.0$ MHz, $e^2Qq/h = 3$ MHz, $\eta = 1$ and $\beta',\gamma' = 0, 0°$, as shown in Figure 6b. The same quality fit was obtained with $\beta',\gamma' = 60, 275°$ and $\eta = 0.2$ which are closer to the DFT predictions, but (A_{xx},A_{yy},A_{zz}) had to be reduced to (5, 5, 6.5) MHz. We assign these signals to N_{eq} which is expected to have a lower coupling than N_{ax}. The calculated spectrum shows, in addition to the strong (dq,dq) cross-peaks, also ridges corresponding to the single quantum (sq) transitions. The absence of the sq type cross-peaks in the experimental spectrum is due to their relative low intensity. Increasing the minimum contour level, similar to the relative value in the experimental spectrum, will practically eliminate them. Calculations of the HYSCORE spectrum with the DFT parameters of N_{eq} of the optimized structure (Table 3) produced the spectrum presented in Figure 6c. The location of the (dq,dq) peaks, appearing at (11.4,7.6) MHz, deviates significantly from the experimental results. The DFT values obtained from the crystal structure exhibit a rather wide range, all with an anisotropy larger than that found by the HYSCORE simulations (see below).

To obtain a set of hyperfine and quadrupole parameters that reproduce the ENDOR spectra at both X- and W-band, we have simulated all spectra using as initial values the parameters predicted by the DFT calculations, given in Table 3, and those obtained from the HYSCORE simulations. While the nuclei within the N_{ax} and N_{eq} groups are practically chemically equivalent in the optimized structure, in the crystal structure they exhibit large differences, especially within the N_{eq} group. The N_{ax} best fit simulated spectra[56] that reproduced both the field dependence of the W-band spectra and the line positions of the X-band spectra are presented as solid black lines in Figures 4 and 5, and the parameters obtained are listed in Table 3 as N_{ax}(exp). The simulations show that signals are also expected at the 0−5 MHz range, which were not detected in the experimental spectra. The absence of these signals is attributed to difficulties in observing ENDOR signals at very low frequencies. In general the fit parameters show a good

(56) The so-called "best fit" simulated spectra were obtained by interactive "eye fitting" simulation searching for the parameters that reproduce best the experimental spectra, rather than by an automated least-squares analysis.

agreement with the DFT values. There is a very good agreement for A_{xx} and A_{yy}, β,γ, e^2qQ/h, and β. The value of A_{zz} is smaller by about 10−15% from the various calculated values. The DFT value of η is more scattered than any of the other parameters, ranging between 0.0 for the optimized structure to 0.11 and 0.27 in crystal structure. The best fit value was found to be on the higher side, 0.3.

In contrast to N_{ax}, which showed a clear signal in both X- and W-band ENDOR spectra with some distinct orientation dependence in the latter, the signals of N_{eq} were not as conspicuous. Therefore we did not attempt to simulate them but rather calculated the spectra using the DFT calculated parameters, listed in Table 3, for the optimized and crystal structures and also for the values obtained from the HYSCORE simulations. The calculated W-band spectra are shown in Figure 4 (traces a, b, and c) compared with the experimental spectrum. The crystal values generated a doublet centered at the ^{14}N Larmor frequency, 10 MHz, and each component is rather broad. The position of the high-frequency component agrees with the position of the broad, 13 MHz peak in the experimental spectrum. The low-frequency component of the doublet in the calculated spectrum is centered at ∼7 MHz, and the experimental spectrum exhibits a broad weak line at this position. The spectrum generated from the optimized structure parameters appears in the same frequency region, but with narrower lines. The same behavior is found for the spectrum calculated using the HYSCORE simulation values. The A_{xx} (A_{yy}) values of the latter are close to the value of the optimized structure and the average value of the crystal structure (4.7 MHz); the calculated A_{zz} value is however somewhat overestimated (by 24−28%).

Comparison of the experimental X-band ENDOR spectra with calculated spectra of N_{eq} obtained with the DFT values of the optimized and crystal structures, with the values obtained from the HYSCORE simulations, are shown in Figure 5. All calculated signals appear within the 0−5 MHz range where some weak signals are apparent in the experimental spectra. The width of the N_{eq} signals in the experimental spectra, primarily in the W-band spectra, suggests a distribution of parameters, although smaller than predicted by the crystal structure. As in the case of N_{ax} the DFT calculation overestimates A_{zz} by about 15−25%.

This comparison of the calculated N_{eq} spectra with the experimental X- and W-band spectra shows that the DFT calculation predicts rather satisfactorily the hyperfine and quadrupole tensors.

Proton Hyperfine Interactions. Considering the structure and symmetry of the complexes (see Figure 1) the protons of Cu_2RGT can be divided into four groups: (i) 6 NH protons which are exchangeable, (ii) 12 methylene protons, termed *c*, bonded to two N_{eq}, each coordinated to a different Cu ion, (iii) 12 methylene protons, bound to an $HN_{eq}(CH_2)_2$ on one side and a CH_2 on the other, termed *b*, and (iv) 12 methylene protons bound to a CH_2 on one side and an $N_{ax}(CH_2)_3$ on the other, termed *a*. In Cu_2GT the NH protons are missing and the 12 *c* type are replaced by six protons termed *c*′ due to the double bond. The *a* and *b* types are similar to those of Cu_2RGT, and we term them *a*′ and *b*′. The protons within each methylene are not necessarily chemically equivalent, and therefore their hyperfine couplings can be different as indeed predicted by the DFT calculations. Thus, in principle, we can have up to seven different types of protons for Cu_2 RGT, while those with a large a_{iso} will be the easiest to resolve. The DFT calculations, carried out using the crystal and the optimized structures, predict a significant a_{iso} for the NH protons and for one of each of the methylene protons of *a* and *c*. Similarly, it predicts large a_{iso} values for *c*′ and one of the *a*′ methylene protons in the Cu_2GT complex. These are listed in Tables 4, 5. All other protons in all structures gave $|a_{iso}| < 1$ MHz and therefore are not expected to be resolved.

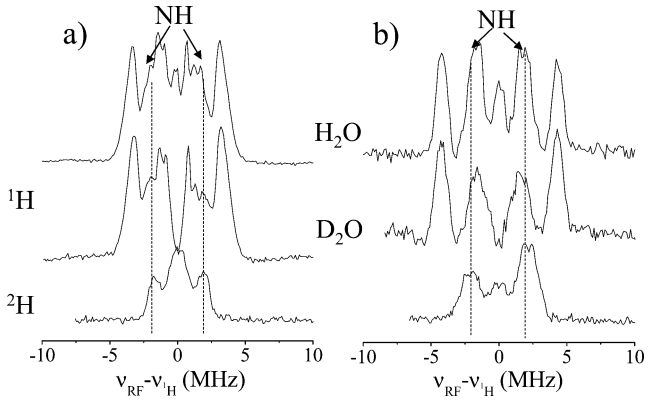

Figure 7. W-band ^{1}H Davies and ^{2}H Mims ENDOR spectra of Cu_2RGT in H_2O and D_2O recorded at $g_\perp$ (a) and $g_\parallel$ (b). The scale of the ^{2}H spectra was multiplied by $\gamma_{^1H}/\gamma_{^2H}$, and the intensity by −1 to ease the comparison. The dotted lines mark the frequencies of the NH protons.

The DFT results were used as guidelines in the analysis of the ^{1}H ENDOR spectra, where we have concentrated on the resolved protons. We begin the analysis with the NH protons because they can be readily isolated by measuring the ^{2}H spectrum of D_2O exchanged samples.

NH Protons of Cu_2RGT and the Orientation of $g_\parallel$. Figure 7 compares the W-band ^{1}H Davies spectra of the Cu_2RGT complex in H_2O and D_2O along with the ^{2}H Mims ENDOR spectra of the latter. The $g_\perp$ spectrum (Figure 7a) of the D_2O solution shows a reduced intensity in the region of ±(1.5−2.2) MHz as compared to the H_2O spectrum. The ^{2}H spectrum exhibits a doublet with a splitting of 3.8 MHz in the proton frequency scale, and there is a relatively broad peak at the Larmor frequency at the center of the spectrum. Similarly, the spectrum recorded in the $g_\parallel$ region shows that the NH protons contribute in the ±2 MHz region, overlapping with other nonexchangeable protons. Comparison with the ENDOR spectra of Cu_2GT in H_2O/D_2O, where the NH proton is absent, shows that a major fraction of the signal in the ^{2}H Cu_2RGT/D_2O spectrum is indeed due to the ND and not D_2O.

The orientation selective ^{2}H Mims ENDOR spectra of Cu_2RGT/D_2O are presented in Figure 8. It shows that as $g_\parallel$ is approached the doublet splitting increases to 4.2 MHz and the intensity in the center of the spectrum has reduced significantly. This reduction indicates that, in addition to contribution from matrix deuterons, the signal at the Larmor frequency in the $g_\perp$ spectrum has considerable contributions from the ND deuterons. At $g_\parallel$ the spectrum is well resolved, with a 140 kHz quadrupolar splitting ν_D within each doublet component. At this particular field position the spectrum is single-crystal-like, and therefore ν_D can be used to estimate the orientation of the N−D bond with respect to $g_\parallel$ using the relation:

$$\nu_D = (3e^2Qq/4h)[3\cos^2\beta' - 1] \qquad (2)$$

Table 4. Simulation Parameters for the ^{1}H ENDOR Spectra of Cu_2RGT as Compared with the Values Obtained from the DFT Calculations; for the NH Proton the Parameters Obtained from the Point−Dipole Approximation Are Also Given

type	ρ(Cu)	T_{xx}, MHz	T_{yy}, MHz	T_{zz}, MHz	a_{iso}, MHz	β (deg)
N−H, exp.		−0.7	−1.6	2.3	−3.6	82
point−dip.	0.20	−1.00	−1.4	2.38		102
DFT, RGT crys.[a]	0.33	−1.72	−3.18	4.91	−1.98	92.3 (96.5)[b]
DFT, RGT opt.	0.33	−1.58	−2.71	4.30	−1.92	80.5 (99.5)
b, exp.		−2	−2	4	0	20
a, exp.		−0.7	−0.7	1.4	7.3	25
DFT, RGT cryst.[a]	0.33	−1.0 ± 0.1	−1.5 ± 0.1	2.5 ± 1	7.9 ± 1 (21.3 ± 4)[c]	34.3
DFT, RGT,opt.	0.33	−0.87	−1.31	2.18	11.73	32.9
c, exp.		−0.4	−0.55	0.95	3.2	90
DFT, RGT cryst.[a]	0.33	−0.6 ± 0.1	−1.1 ± 0.1	1.7 ± 0.1	3.7 ± 0.7	87
DFT, RGT opt.	0.33	−0.49	−1.03	1.53	4.2	83.4 (96.6)

[a] The values were averaged and show a considerable spread over the six protons. [b] The value in parentheses shows the angle for the same type of proton in a different, symmetry-related location in the molecule. [c] Here the protons were divided into two main groups of 4 and 2 (in parentheses), with significantly different a_{iso} values.

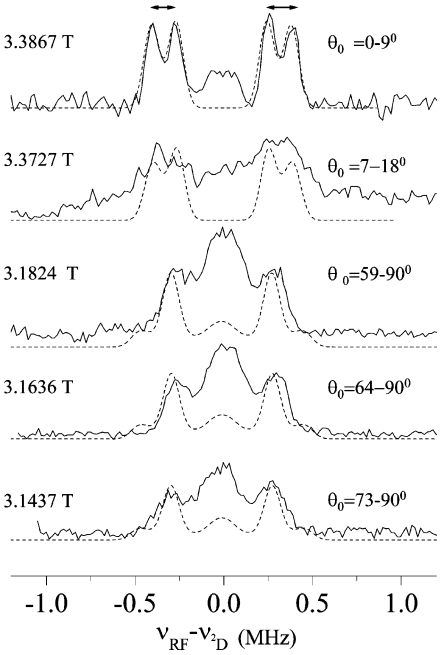

Figure 8. Field dependent ^{2}H-Mims W-band ENDOR spectra of Cu_2RGT/D_2O and the corresponding simulations (dashed lines) obtained with the parameters listed in the text. The magnetic field positions at which the spectra were recorded and the selected θ_0 orientations are listed in the figure. For convenience the intensity was multiplied by −1. The arrows at the top spectrum mark the quadrupole splitting.

In eq 2 β' is the angle between the principal Z axis of the quadrupole interaction, Z_p, and the magnetic field. The asymmetry parameter, η, was neglected in eq 2 because it is relatively small.[57,58] Taking the quadrupole coupling constant (e^2Qq/h) of the ND deuterons as 210 kHz[57,58] $\beta' = 79°$ is obtained. The angle between the NH bond and the Cu−Cu direction in the crystal structure is 89°, which is in a good agreement with the experimental value, considering the uncertainty in e^2Qq/h and the assumption that $\eta = 0$. This provides experimental evidence for $g_{||}$ being along the Cu−Cu direction as expected for the trigonal bipyramidal coordination geometry of the copper ions, in agreement with the DFT calculations (see above).

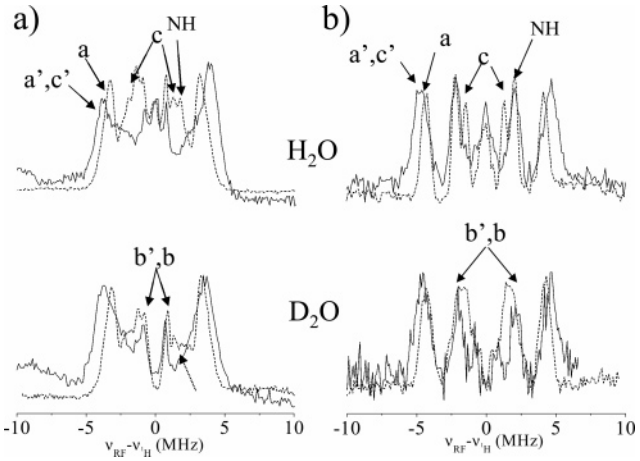

Figure 9. W-Band ^{1}H ENDOR spectra of Cu_2GT (solid lines) and Cu_2-RGT (dashed lines) recorded at (a) $g_\perp$ and (b) $g_{||}$ in H_2O (upper trace) and D_2O (lower trace).

Using the quadrupolar tensor parameters listed above as starting values the W-band ^{2}H orientation selective spectra of Cu_2RGT/D_2O were simulated (see Figure 8). The best fit hyperfine and quadrupole tensor parameters were: (A_{xx},A_{yy},A_{zz}) = (−0.8,−0.66,−0.2) MHz, (β,γ) = 82°,90°, e^2Qq/h = 220 kHz, η = 0.14, and (β',γ') = 90°,82°. This translates to an isotropic hyperfine coupling, a_{iso}, of ∓3.6 MHz and anisotropic principal components (T_{xx},T_{yy},T_{zz}) = (∓0.7,∓1.6,±2.3) MHz for protons. We chose the positive T_{zz} option as would be expected from an interaction which is governed by point−dipole interaction. These ^{1}H hyperfine parameters are compared to the DFT values in Table 4. There is a good agreement in the orientation of T_{zz} with respect to $g_{||}$; the nonaxial nature of the interaction is reproduced, but the magnitude of T_{zz} is overestimated by as much as ∼100% for DFT values. In contrast, a_{iso} is underestimated, but the sign is reproduced.

Other Protons. For further assignment of the proton signals, the W-band Davies ENDOR spectra of Cu_2RGT and Cu_2GT in H_2O and D_2O, recorded at $g_{||}$ and $g_\perp$, were compared, as shown in Figure 9. The $g_{||}$ spectrum of the Cu_2RGT complex exhibits, in addition to the NH signals, two doublets with hyperfine splittings of ∼9 MHz and ∼4 MHz. Comparison of the line widths and the shifts observed for the two complexes suggests that the 9 MHz doublet in the Cu_2GT complex, which is significantly broader than the Cu_2RGT doublet, includes contributions from two types of protons. Similarly, the broader lines

(57) Michal, C. A.; Wehman, J. C.; Jelinski; L. W. *J. Magn. Reson. B* **1996**, *111*, 31−39.
(58) Usha, M. G.; Peticolas, W. L.; Wittebort, R. J. *Biochemistry* **1991**, *30*, 3955−3962.

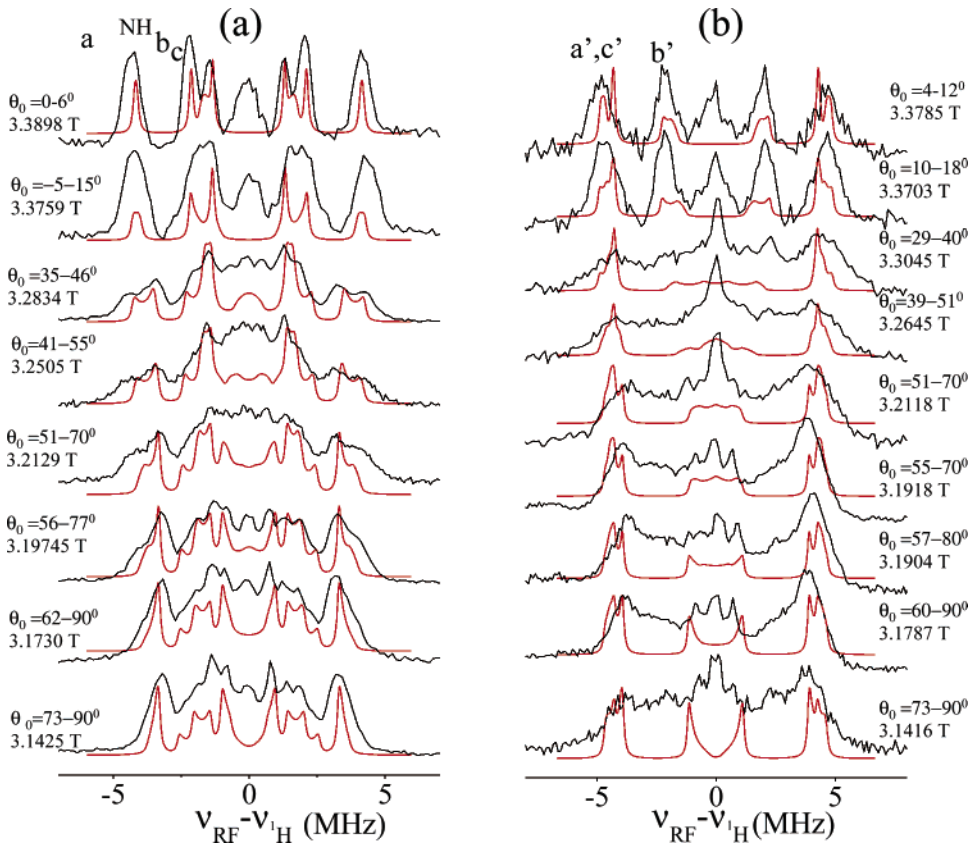

Figure 10. (a) Field dependent ^{1}H-Davies W-band ENDOR spectra of Cu_2RGT/H_2O along with the sum of the simulated spectra of the NH, *a*, *b*, and *c* protons. (b) Same for the Cu_2GT/H_2O and *a*′, *b*′, and the *c*′ protons. The selected θ_0 range and the observer fields are noted on the spectra, and the parameters used for the simulations are given in Tables 4,5.

of the 4 MHz doublet for the Cu_2RGT complex (see the D_2O spectrum) indicate that it originates from two types of protons. Accordingly, we assign the signals of protons *a*′, *c*′ of Cu_2GT to the ∼9 MHz doublet and proton *b*′ to the ∼4 MHz doublet. In Cu_2RGT proton *a* has a hyperfine coupling of 8.6 MHz, while protons *b* and *c* have couplings of ∼4 MHz. The major differences between the spectra of Cu_2GT and Cu_2RGT recorded at $g_\perp$ are the increased width of the ∼9 MHz doublet and the outward movement of intensity at ±2 MHz (see low dotted arrow in Figure 9a). The assignment of the Cu_2RGT *c* and Cu_2GT *c*′, as noted on the figure, stemmed from the expectation that their hyperfine couplings should change due to the introduction of the double bond in Cu_2GT (see Figure 1). The assignment of *a* and *b* relied on the DFT prediction that proton *a* should have a significantly larger a_{iso}. This leaves the *b* protons as an effective representative of protons with a significant anisotropic interaction but small a_{iso}.

The series of the orientation selective spectra of Cu_2RGT presented in Figure 10a shows that proton *a* is resolved throughout the series and exhibits a large a_{iso} but a rather small anisotropy. To further determine the extent of the anisotropy and to resolve the overlapping powder patterns at $g_\perp$, we have carried out a 2D TRIPLE experiment, which generates correlations between ENDOR lines belonging to the same electron-spin manifold.[27] The ^{1}H 2D TRIPLE spectrum is symmetric with respect to $\nu_{^1H}$, and for a system with two protons with ENDOR frequencies $\nu_{1\alpha}$, $\nu_{1\beta}$, $\nu_{2\alpha}$, and $\nu_{2\beta}$, it exhibits four cross-peaks at ($\nu_{1\alpha}$,$\nu_{2\alpha}$), ($\nu_{2\alpha}$,$\nu_{1\alpha}$), ($\nu_{1\beta}$,$\nu_{2\beta}$), and ($\nu_{2\beta}$,$\nu_{1\beta}$). The 2D TRIPLE spectrum of Cu_2RGT/D_2O is depicted in Figure 11a. The diagonal of the spectrum, which represents the corresponding ENDOR spectrum, has three pairs of peaks at ±3.2, ±1.3, and ±0.8 MHz, assigned to protons *a*, *c*, and *b*, respectively. The +1.3 MHz peak has a significantly lower intensity than its −1.3 MHz counterpart. Cross-peaks appear at (−3.2,−1.3) (−1.3,−3.2), (−3.2,0.8), (0.8,−3.2), (−1.3,0.8), and (0.8,−1.3), corresponding to only one of the electron-spin manifolds of (*a*,*c*), (*c*,*a*), (*a*,*b*), (*b*,*a*), (*c*,*b*), and (*b*,*c*), respectively. All the other six peaks, representing the other spin manifold, are missing. This is attributed to the low *S*/*N*. The reason for this low intensity, compared to the −1.3 MHz counterpart, is, however, not clear. The 2D TRIPLE was recorded several times, and the same spectrum was obtained each time. Nonetheless, because of the symmetry of the 2D TRIPLE spectrum, the information content of the missing peaks is redundant. The location of the (*a*,*c*) peak in the (−,−) quadrant shows that the hyperfine

Table 5. Simulation Parameters for the ENDOR Spectra of Cu_2GT as Compared with the Values Obtained from DFT Calculations

type	ρ(Cu)	T_{xx}, MHz	T_{yy}, MHz	T_{zz}, MHz	a_{iso}, MHz	β (deg)
b′, exp.		−2.3	−2.3	4.6	0	15
a′, exp.		−0.7	−0.7	1.4	8.5	25
DFT, GT cryst.[a]	0.34	−0.9	−1.7	2.6	13.6	30.1
DFT, GT opt.	0.32	−0.9	−1.5	2.4	15.9	35.1
c′, exp.		−0.3	−0.3	0.6	8.8	70
DFT, GT cryst.[a]	0.34	−0.38	−1.38	1.76	3.02	83 (96)[b]
DFT, GT opt.	0.32	−0.33	−1.05	1.38	4.28	84 (96)

[a] The values for the six protons were practically the same. [b] The value in parentheses shows the angle for the same type of proton in a different, symmetry-related location in the molecule.

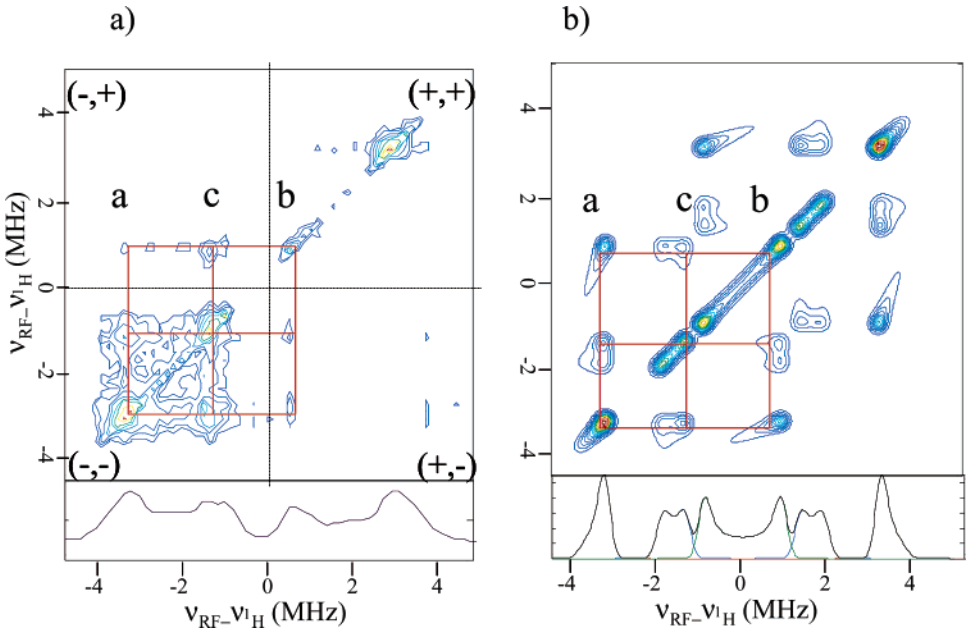

Figure 11. (a) W-band 2D $^1H-^1H$ correlation difference TRIPLE spectrum of Cu_2RGT/D_2O recorded at 8 K at $g_\perp = 2.139$. (b) The simulated $^1H-^1H$ correlation difference TRIPLE spectrum. The parameters used for the simulations are given in Table 4.

couplings of *a* and *c* have the same signs. Moreover the spread of their ridges is rather small. The (*a*,*b*) and (*c*,*b*) cross-peaks appear in the (−,+) and (+,−) quadrants, and therefore the sign of the hyperfine coupling of *b* is different than that of *a* and *c*. The 2D TRIPLE results thus provide additional constraints on the spin-Hamiltonian parameters, and the best fit parameters should reproduce both the ^1H and ^2H orientation selective ENDOR spectra and the 2D TRIPLE spectrum. The simulated 2D TRIPLE spectrum obtained with such parameters is shown in Figure 11b, and the values used for the simulations are given in Table 4.

Orientation selective ENDOR spectra of Cu_2RGT/H_2O and their simulations are depicted in Figure 10a. The latter includes the NH proton as well (a similar series from the D_2O solution was recorded but is not shown). In these simulations the initial α, β, and γ values were taken from the DFT calculations. These were usually found to be similar to those calculated using the point−dipole approximation and the crystal structure coordinates, as described in refs 17, 24. The simulations were most sensitive to β, and therefore this value is listed in Table 4. Except for the NH proton, the hyperfine values of proton *a* have the highest accuracy because its signals are relatively well resolved throughout the orientation selective series. The determination of the parameters of proton *b* is less unique because of its overlap with the *c* signals and its proximity to the Larmor frequency in the $g_\perp$ region. We finally note that although the measurements were carried out at W-band, the orientation selectivity in the $g_\perp$ region is rather poor due to the splitting to seven[63,65] Cu hyperfine components. For example, the spectra recorded in the field range 3.1425−3.1729 T were very similar.

The orientation selective spectra of Cu_2GT are less resolved than those of Cu_2RGT due to the overlap of the signals of *a*′ and *c*′, and consequently their simulations are not unique. In addition, we were not able to obtain 2D TRIPLE spectra with reasonable quality. Initially we assumed that the hyperfine parameters of *a*′ and *b*′ are the same as those of *a* and *b* of Cu_2RGT and tried to simulate the orientation selective ENDOR spectra of Cu_2GT just by fitting the hyperfine parameters of *c*′. This gave a T_{zz} value that was significantly larger than that of proton *c* in Cu_2RGT, which is inconsistent with the crystal and DFT structures. Moreover, the value of β was found to be 0°, again too far from DFT value of 83°−84°. Hence, we relaxed the constraint that protons *a* and *a*′ have the same a_{iso} value and allowed for a slight increase in a_{iso} while keeping β close to the DFT value and T_{xx}, T_{yy}, and T_{zz} close to the values of *c*. The resulting simulations are shown in Figure 10b, and the parameters are listed in Table 5. The simulations of this series also helped to refine the parameters of *b* and *b*′ because the *b*′ and *c*′ signals do not overlap in these spectra. While simulating the spectral feature of the *b*, *b*′ protons, we restricted ourselves to small a_{iso} values as predicted by the DFT calculations.[59] In the simulations shown in Figure 10a,b we concentrated on reproducing the line positions and not the line width, and therefore we did introduce strain effects and extra line width.

Finally to identify any contributions from the Cu(II) impurity, the ENDOR spectrum of the sample that has been deliberately decomposed was measured as well. The spectrum measured at $g_\perp = 2.02$ showed a typical spectrum of a Cu(II) with water ligands with the $A_\perp$ singularities appearing at ±1.5 MHz, superimposed on a broad background. The spectrum recorded at $g_\parallel$ was very poorly resolved; thus none of the features observed in the ^1H spectra of the Cu_2RGT and Cu_2GT complexes are due to the Cu(II) impurity.

Comparison with the DFT predictions listed in Tables 4 and 5 show that while the introduction of the double bond in Cu_2-GT led to an increase of about 100% in the experimental a_{iso} of proton *c*′ compared to *c* in Cu_2RGT, the DFT calculations predicted no change. Nonetheless, the small increase in a_{iso} predicted for *a*′ compared to *a* was observed also experimentally. As observed for the NH protons, also the other protons show a good agreement in the orientation of the hyperfine interaction,

(59) DFT values are not listed in Tables 4 and 5 for protons *b* and *b*′ since they cannot be assigned to specific protons, because there are too many weakly coupled protons.

but the magnitude of the anisotropic hyperfine components, T_{ii}, is consistently overestimated by a factor of about 2 compared to the simulation values.

Discussion

The choice of the specific Cu_2RGT and Cu_2GT binuclear complexes along with the application of a variety of EPR techniques that allowed us to probe a relatively large number of magnetic interactions at different sites of the molecules provided a unique opportunity to evaluate the role DFT calculations can play as a major component of the EPR data analysis tool box. It also helped to clarify the strengths and weaknesses of DFT calculations in terms of predicting magnetic tensors, once the optimized structure is a good representation of the real solution structure. The latter conclusion was derived from the good agreement between the experimental **g** and Cu hyperfine parameters for both complexes. This is supported by the rather close values obtained from calculations of the magnetic tensors using the atomic coordinates of the crystal and optimized structures. This also indicates that the solution structure is close to the crystal structure, as expected for the rigid structures of the two complexes.

The agreement between the experimental and calculated *g* tensors for the Cu_2RGT and Cu_2GT complexes is significantly better than that usually obtained for mononuclear Cu(II) complexes.[38,39] A similar behavior was previously noted for the Cu_A.[14] A reasonable explanation for this discrepancy between mononuclear Cu(II) and delocalized mixed-valence Cu(1.5)-Cu(1.5) complexes is the shape of the DFT exchange hole. It is well-known that this hole is too delocalized relative to the exact hole and always favors delocalization over localization. It can also be thought of as a consequence of the self-interaction error which also leads to overdelocalization. Thinking either way, it appears to us reasonable to expect that DFT works better for an inherently delocalized system such as the present one compared to less delocalized mononuclear Cu(II) centers. It would, however, be difficult if not impossible to infer the nature of a delocalized versus localized bonding situation from DFT alone since it will always be in favor of delocalization. This tendency diminishes with increasing amounts of Hartree−Fock exchange in the DFT functional, while, ultimately, the Hartree−Fock method itself is biased in favor of localized descriptions.

Within varying levels of accuracy, the magnitude and orientation of the hyperfine and quadrupole tensor of N_{ax} and N_{eq} and the hyperfine tensor of the NH, *a*, and *c* protons of Cu_2RGT were determined. In addition the orientation of $g_{||}$ was shown experimentally to be along the Cu−Cu direction, as expected. For Cu_2GT the hyperfine interactions of protons *a*′ and *c*′ were obtained. The DFT predictions were particularly good guidelines in the analysis of the broad lines in the W-band ^{14}N ENDOR spectra, and they prompted additional X-band ENDOR and HYSCORE measurements. In addition, they confirmed the assignment of the different ^{14}N signals to N_{eq} and N_{ax}. The DFT calculations predicted rather well the nitrogen hyperfine and quadrupolar couplings with the main deviations being in A_{zz} (20−30%).

For the ^{1}H hyperfine interactions the correlation between the experimental and DFT results is more complex. The DFT calculations were most instrumental in terms of the assignment of the strongly coupled protons and in providing some constraints for the simulation of the weakly coupled protons exhibiting clear lines in the ENDOR spectrum, namely protons type *b* and *b*′ for which a_{iso} had to be kept small. The DFT calculated β value of the principal hyperfine direction was found to be close to the experimental values for all protons. The calculations also successfully predicted the number of protons with large a_{iso} values and the a_{iso} sign, but in terms of absolute a_{iso} values the agreement was not always satisfactory and variations of up to ±100% were observed. For proton *c* the agreement was very good; for *c*′ and the NH, a_{iso} was underestimated, whereas, for *a* and *a*′, it was overestimated. These discrepancies are attributed the large ^{1}H gyromagnetic ratio which makes the hyperfine couplings highly susceptible to minute changes in the spin populations, which are within the error of the current state of the art of the DFT methodology. A single spin in the H-1s orbital leads to a hyperfine coupling of about 1400 MHz. Thus, the a_{iso} values measured in this work for even the "strongly" coupled protons only represent a few ppt of the spin population. It is evident that such small numbers are difficult to predict to high accuracy. Besides, one might expect significant effects from vibrational averaging for proton hyperfine coupling, which for molecules of the size studied in this work is impractical to evaluate.

The considerable difference in the DFT calculated a_{iso} of the two methylene protons of *a* and *a*′ stems from the different orientations of the C−H bonds with respect to the Cu−Cu orientation. The latter determines the degree of overlap with the singly occupied MO, which has to a large extent a d_{z^2} character such that the protons with the C−H bond more parallel to the Cu−Cu axis have a significantly larger a_{iso} value (see Figure 2). Also in the case of the *c* proton only one of the methylene pair has a large coupling, which arises from the fact that the partner proton is necessarily quite remote from the bulk of the spin population and can not, therefore, pick up enough spin density leading to discernible signals. We found rather surprising the indifference of the DFT results to the introduction of the double bond in one of the N−C−C−N bridges, namely the prediction that the couplings of *c* and *c*′ are the same. This stems from the vanishing spin density on the CH−CH or CH_2−CH_2 bridges and the similar orientation of the C−H bond with respect to the Cu−Cu direction for the *c* and *c*′ protons in the calculated structure. The observed experimental change suggests that some structural variation is present in the real solution structure.

The rationale for the large coupling of the NH protons is their vicinity to the unpaired spin which significantly delocalizes onto the nitrogen ligands (2−4% onto the equatorial ligands). This leads to relatively large isotropic couplings through spin polarization of the N−H bonds as well as reasonably large dipolar couplings through interaction of the proton nuclear spin with the unpaired spin population on the nitrogen nucleus.

The DFT calculated T_{ii} values of both optimized structures and crystal structures in Cu_2RGT and Cu_2GT were found to be consistently larger than the experimental values by ∼100%. The anisotropic part of the proton hyperfine interaction, **T**, can be estimated from the crystal structure using the point−dipole approximation[17,24] and the spin distribution. Therefore a comparison of the experimental and calculated **T** can, in principle, be used to estimate spin distribution, as we have shown in the case of the mixed valence binuclear Cu_A center in a number of

proteins.[17] This approach assumes that the structure solution of the complex is similar to that of the crystal, which may not always be true, but in the case of Cu_2RGT and Cu_2GT it is a reasonable assumption. Another point of concern is that the protons' distance from centers with large spin populations should be large enough (>2.5 Å). For example, if there are a substantial spin populations on N_{eq}, its contribution to **T** of the NH protons cannot be described by the point−dipole approximation due to the short N−H distance. Nevertheless, with these limitations in mind, the comparison of the point−dipole **T** calculations and experimental values does provide some insight, especially when DFT results are not available. While the principal components of **T** strongly depend on the spin density distribution, the orientation shows only a subtle dependence, provided that the spin populations on all nuclei other than the Cu are small. Thus a good agreement between the experimental and calculated values indicates that the solution structure is not significantly different from the crystal structure.

We first calculated the T'_{ii} and β values of the NH proton of Cu_2RGT using the point−dipole approximation. The best agreement with the experimental values was obtained by setting $\rho_{cu} = 20\%$ as listed in Table 4. Adding $\rho_{N_{eq}} = 1-2\%$ did not increase the values significantly, while N_{ax} was found to be too far and therefore $\rho_{N_{ax}}$ was neglected. A spin population of 20% on each of the copper nuclei is too low compared to the DFT value of 33% and the value predicted using eq 1, e.g., 38−39%. This implies that the point−dipole approximation does not apply for the short N−H distance, although the spin population is small but probably significant enough. Next we considered the *a* methylene; the calculated T_{ii} values of the two methylene protons are different, both yielding an axial **T** for $\rho_{N_{ax}} = 0$, where for one of them $\rho_{cu} = 0.22$ reproduces the experimental results. Setting ρ_{Cu} and $\rho_{N_{ax}}$ to the DFT values yielded similar values to those reported by the DFT calculations, but significantly larger than the experimental values. Similarly, the point−dipole approximation calculations for one of the *c* proton yields a good agreement with the experimental value only for $\rho_{cu} = 0.22$. The same trends were observed for the protons of Cu_2GT. This comparison shows that the spin population obtained from the comparison with the experimental data should be handled with care.

Finally we note that although the azacryptate ligands stabilized the mixed-valence state of the two coppers with one unpaired electron delocalized over the two coppers, the electronic structure of these complexes is very different from that of the binuclear Cu_A center. Here most of the spin population is on the Cu, and some is also found on the two axial N_{ax} due to the direct overlap of its p_z with the d_{z^2}. The N−C−C−N bridges were found to have negligible spin densities as suggested by earlier Raman investigations.[10,14]

Conclusions

The solution spatial and electronic structure of binuclear mixed-valence copper azacryptate complexes were determined using an integrated EPR/ENDOR/HYSCORE/DFT calculation approach. The DFT calculations were found to be a most useful element in the spectral interpretation. For these specific complexes, which are rigid and have a delocalized character, DFT gave a good prediction of the **g** and Cu hyperfine interaction. A satisfactory agreement was obtained for the ^{14}N hyperfine and quadrupole interactions for the optimized structure. For ^{1}H a very good agreement was found for the hyperfine tensor orientation, signs, and trends in terms of relative magnitudes. All these are very useful for the assignment of the ENDOR signals and as constraints on the best fit simulations. While the anisotropic hyperfine components were found to be consistently overestimated (by ∼100%), the isotropic part showed similar deviations but not systematically. Although the DFT still suffers from shortcomings, it has reached a state where it can be carefully integrated into the analysis process, especially in the case where spectra are complex. It provides guidelines and starting values for simulations when many tensors are involved.

Acknowledgment. This work has been supported by the German-Israel Foundation for Scientific Research (D.G. and F.N.). We thank Dr. Boris Epel for providing us with the Kazan tool box and for teaching us how to use it. D.G. also thanks Peter M. H. Kroneck for bringing to her attention the existence of these compounds and for making the initial contacts.

Supporting Information Available: The X-ray determined structures and the structures and coordinates of the optimized $[Cu_2GT]^{3+}$ and $[Cu_2RGT]^{3+}$. This material is available free of charge via the Internet at http://pubs.acs.org.

JA056207F